Antarct. Meteorite Res., **11**, 103–121, 1998

SEARCH FOR ^{60}Ni EXCESSES IN MET-78008 UREILITE: AN ION MICROPROBE STUDY

Noriko T. KITA[1], Shigeko TOGASHI[1], Yuichi MORISHITA[1], Shigeru TERASHIMA[1] and Hisayoshi YURIMOTO[2]

[1]*Geological Survey of Japan, 1–3, Higashi 1-chome, Tsukuba, Ibaraki 305-8567*
[2]*Department Earth and Planetary Science, Faculty of Science, Tokyo Institute of Technology, 12–1, Ohkayama 2-chome, Meguro-ku, Tokyo 152-8551*

Abstract: We have developed a technique for *in-situ* Ni isotopic analysis using the ion microprobe, in order to detect ^{60}Ni excess from the decay of the short lived nuclide ^{60}Fe (half life=1.5 Ma) in ureilite samples. The silicate minerals from MET-78008 ureilite with an old U-Pb age of 4.563±0.006 Ga were analyzed. The ^{56}Fe/^{58}Ni ratios of olivine and orthopyroxene are between 2700 and 5400. In spite of the high Fe/Ni ratios, we could not observe any detectable ^{60}Ni excess. From the mean value of olivine core data, we obtain an upper limit of the ^{60}Fe/^{56}Fe ratio at the time of ureilite formation of 1.8×10^{-7}. The time difference between CAI formation and ureilite formation was estimated to be more than 4 million years, which is consistent with the U-Pb data from the same meteorite. We concluded that the impact event for the disruption of the ureilite parent body happened more than 4 million years after CAI formation. However, a large uncertainty in the initial ^{60}Fe/^{56}Fe ratio is introduced by the possibility that the ^{60}Ni excess observed in CAIs is of nucleosynthetic origin. Our conclusion may change if the initial ^{60}Fe/^{56}Fe ratio of the solar system using CAI data is too high.

1. Introduction

Most ureilites consist of olivine and pigeonite with carbon-metal veins. This ultramafic mineralogy of ureilites limited the information on their formation ages because they do not contain any significant amounts of U-Th, REE, and alkali elements for precise age determination (GOODRICH, 1992; TORIGOYE-KITA *et al.*, 1995a). An exception is the Ca-rich ureilite MET-78008, which has an old U-Pb age of 4.563±0.006 Ga (TORIGOYE-KITA *et al.*, 1995b). This ureilite contains augite and shows high abundances of trace elements. According to the time difference between CAI formation (4.566±0.002 Ga; MANHÈS *et al.*, 1988) and the formation of MET-78008, the formation of ureilites took place within 10 million years after solar system formation. Ureilites could be as old as other igneous meteorites, such as eucrite and angrites.

The ultramafic mineralogy and highly depleted lithophile element abundances clearly indicate that the ureilite underwent igneous processes (GOODRICH, 1992; WARREN and KALLEMEYN, 1992). On the other hand, ureilites are primitive in terms of their high carbon contents, relatively undepleted siderophile elements (*e.g.*, HIGUCHI *et al.*, 1976), abundant noble gases in the carbon-bearing veins (GÖBEL *et al.*, 1978), and heterogeneous oxygen isotopic compositions which correlate with olivine Mg numbers (CLAYTON

and MAYEDA, 1988). Several ureilites formation models were suggested involving nebular fractionation (CLAYION and MAYEDA, 1988), partial melting events (WARREN and KALLEMEYN, 1992), and planetary collisions (TAKEDA, 1987), though none of the models could fully explain all the features that appear in ureilites (see review by GOODRICH, 1992). In order to understand ureilite formation processes in detail, we need to know the chronology of ureilites on a fine scale.

The discovery of the ^{60}Ni excess from the decay of the short lived nuclide ^{60}Fe (half life of 1.5 Ma) may allow us to determine relative formation ages of ureilites and other meteorite groups. The initial (^{60}Fe/^{56}Fe) ratio of CAIs was estimated to be $(1.6\pm0.5)\times10^{-6}$ (BIRCK and LUGMAIR, 1988). Iron is an abundant element in all classes of meteorites and the (^{60}Fe/^{56}Fe) ratio decreases one order of magnitude every 5 million years, so the ^{60}Fe-^{60}Ni system is suitable for fine chronology of primitive meteorites. A recent bulk analysis of an ureilite by conventional methods could not find any detectable ^{60}Ni excess (SHUKOLYUKOV and LUGMAIR, 1993b). Because the initial ^{60}Fe/^{56}Fe ratio of the solar system was very low and the ^{60}Fe half life is very short, a Fe/Ni ratio of 3000 is required to detect a 1‰ ^{60}Ni excess in the material which formed 5 Ma after the CAI formation. However, Fe/Ni ratios of bulk ureilites are in the order of 100, which is not high enough to detect a small ^{60}Ni excess. Therefore, a mineral with a high Fe/Ni such as a silicate should be analyzed to detect a small ^{60}Ni excess.

In this study, we have developed the technique for the precise Ni isotopic analyses in olivine and low Ca-pyroxene grains using the Cameca IMS-1270 ion microprobe. In-situ micro-analyses using the ion microprobe has the great advantage of analyzing high Fe/Ni phases in the ureilite by avoiding veins, metallic inclusions and thick reduction rims (about 100 μm) containing reduced iron grains. In this work, the ureilite MET-78008 was analyzed. An old U-Pb age of 4.563±0.006 Ga has been obtained for this meteorite (TORIGOYE-KITA *et al.*, 1995b), so that samples from this meteorite are good candidates for detecting an ^{60}Ni excess.

2. Experimental Method

2.1. Preparation of terrestrial standards

We have prepared several olivine and orthopyroxene standards in order to evaluate the analytical procedure. A list of the standards is shown in Table 1. For olivine from Ichinome-gata peridotite nodule (GSJ R57877) and Miyake-Island olivine sands (GSJ M20743), pure olivine grains larger than 1 mm were selected under the binocular microscope. These olivine grains were gently crushed, then a large piece was mounted in epoxy for ion microprobe analysis and the rest of the sample was used for atomic absorption analysis. Olivine from San Carlos was a gem-grade single crystal (2×2×1 cm) and a piece of the specimen was obtained for analyses. Because all these olivine grains are relatively Mg-rich (Fo> 80), more Fe-rich olivines were obtained from Fuji-Hoei Gabbro (Fo=70) and Orikabe Craton (Fo=60). These olivine grains were hand-picked from the 500–1000 μm fraction for Fuji and from the 250–500 μm fraction for Orikabe. For the olivine samples with higher amount of impurity, such as melt inclusions, magnetite and chromite, the smaller grain sized fractions were used for hand pick. We also

Table 1. Terrestrial standards.

Sample	AAA				INAA				
	wt (mg)	Fe%	Ni ppm	Ni/Fe	wt (mg)	Fe%	Co ppm	Ni ppm	Co/Fe
Olivine									
Ichinome-gata	10.5, 13.4	8.0	3047	0.03817	35.83	7.89	151	2978	0.00191
San Carlos	9.91	8.4	2689	0.03197	-	-	-	-	-
Miyake-Island A	12.4	11.2	962	0.00856	-	-	-	-	-
Miyake-Island B	15.6	12.6	787	0.00626	-	-	-	-	-
Miyake-Island C	12.9	12.8	591	0.00463	-	-	-	-	-
Fuji	9.6 - 10.5	19.0	823	0.00433	6.96	19.07	226	*756**	0.00119
Orikabe	9.7	27.1	198	0.00073	13.83	26.70	199	*440**	0.00075
Orthopyroxene									
Ichinome-gata	9.7	5.1	669	0.01314	21.58	5.19	59	660	0.00114

*The INAA Ni data for lower concentrations (<500 ppm) or smaller samples (<10 mg) are not trustful so that they were not used for the ion probe calibration.

collected orthopyroxene grains from the 500–1000 μm fraction of the Ichinome-gata peridotite nodule.

For each sample, Fe and Ni concentrations were measured by atomic absorption analysis. Several rock reference samples (JB-1, JB-2, BE-N, VS-N, UB-N, IF-G, PCC-1, DTS-1) were used for calibration. Both samples and standards of 10 mg weights were dissolved in HF-$HClO_4$ mixture, evaporated to dryness, and dissolved in 10 m*l* 0.1N HCl solution for atomic absorption analyses. Because the Ni concentrations were higher than 100 ppm, Ni was not extracted from the solution and atomic absorption analysis was carried out with the flame method. Deuterium automatic background correction was used for all measurements. We estimate the error of concentration analyses to be 3% using the calibration curve of standard rocks.

Fe, Co, and Ni concentrations were also obtained for some of the standards by INAA. The olivine and orthopyroxene grains weighing 7–36 mg were irradiated in the S-pipe of the JRR-4 reactor at the Japan Atomic Energy Research Institute for 6 hours with a thermal neutron flux of 5.5×10^{13}/cm^2/s. For the INAA standards, comparable amounts of GSJ rock reference sample JB-1 were irradiated simultaneously with the samples. The abundance of Co, Ni and Fe was determined by the high-purity Ge gamma-ray detector (ORTEC GEM20180) of the Geological Survey of Japan (TANAKA *et al.*, 1988). The counting error for Co and Fe was smaller than 1%, while it was 10% for Ni. For the samples with Ni concentrations higher than 500 ppm, Ni analyses were in good agreement with the atomic absorption analyses. Using five separate measurements for JB-1, we found that the reproducibility and accuracy of Co/Fe ratio determinations were within 1%, while the concentrations showed larger variations of 5% for both Fe and Co.

2.2. Condition of ion microprobe analysis

The Cameca IMS-1270 Ion probe used in this study was installed at the Geological Survey of Japan in March 1995. The IMS-1270 is a double focusing secondary ion mass

spectrometer with a 60 cm sector magnet. The design of the secondary ion optics ensures high transmission at a high mass resolution of 6000, which is required for the U-Pb age determination of zircons. In the present study, we used O^- primary ions with an accelerating voltage of −23 kV. The primary ions are focused to a 40 μm diameter beam with homogeneous ion density in order to create a flat bottom sputtered crater. The primary ion intensity was between 25 and 30 nA during the isotope analyses and 5 nA for concentration analyses. Samples were mounted in epoxy, polished, and coated with Au (200 nm thickness). Positive secondary ions were accelerated through 10 kV, which is applied to the sample surface.

The sputtering rate of the sample surface was estimated from the depth analyses of sputtered crater using a stylus-based surface profiler TENCOR P-10. It was 0.05 μm/min for a primary ion intensity of 30 nA. The Ni useful yield defined by SLODZIAN (1975) was calculated to be 0.5% by comparing the number of ions detected by the mass spectrometer during the isotopic analyses and the amount of Ni sputtered from the sample. This value is much larger than that obtained by thermal ionization, 0.05% reported by SHUKOLYUKOV and LUGMAIR (1993b).

A typical Ni mass spectrum of ureilite olivine is shown in Fig. 1. Although Ni has 5 isotopes, ^{58}Ni, ^{60}Ni, ^{61}Ni, ^{62}Ni, and ^{64}Ni, we did not measure ^{58}Ni and ^{64}Ni which have isobaric interference from ^{58}Fe and ^{64}Zn. Molecular interferences from Ca, Sc, and Ti oxides are relatively large compared to the Ni isotopes, because of low Ni concentrations. In order to analyze Ni isotopic ratios with a precision of better than 1‰, it is necessary to reduce any tailing effects from these molecular ions at the Ni isotope masses. It is also necessary to reduce the contribution from hydride interferences. Although the intensities of hydrides are small compared to the Ni isotope signals, the mass difference between hydrides and Ni isotopes are so small (less than 0.01 amu) that high mass resolution is required for separating them. For these reasons, we tuned the secondary ion optics in a manner that mass resolutions at 10%, 1% peak heights become 4500 and 4000, respectively. Tailing of mass peak of ^{57}Fe at a mass 0.02 amu lower than ^{57}Fe was monitored in order to estimate the effects of molecular interference of Ca, Sc, and Ti oxides to the neighboring Ni isotopes. The level of the tailing is about 10 ppm. Among the samples we measured, the ureilite orthopyroxene showed the highest ratio of each oxide signal to the neighboring Ni isotope signal. However, the ratios were as high as 30, so that the effect of molecular interference on the Ni isotopes was less than 0.03%.

The slits and apertures in the secondary ion optics were selected as follows; entrance slit width=75 μm, contrast aperture=400 μm diameter, field aperture=2000 μm square, energy slit lower edge=−25 V, energy slit width=75 V, and exit slit width=180 μm. The field aperture is located at the entrance of the electrostatic analyzer, where the sample ion image (40 μm diameter) is focused with a magnification of 100 (4000 μm diameter). Therefore, a 2000 μm square field aperture restricted the image of sample region to a 20 μm square at the center of the sputtered crater. The entrance slit width of 75 μm reduced the number of secondary ions by 50%. As a result, the transmission of secondary ions is about 25%. This value is smaller than the specification of IMS-1270 on the maximum transmission of 90% at a mass resolution of 5000 (defined by 10% peak height). However, we found that tuning for higher transmission increased the tail-

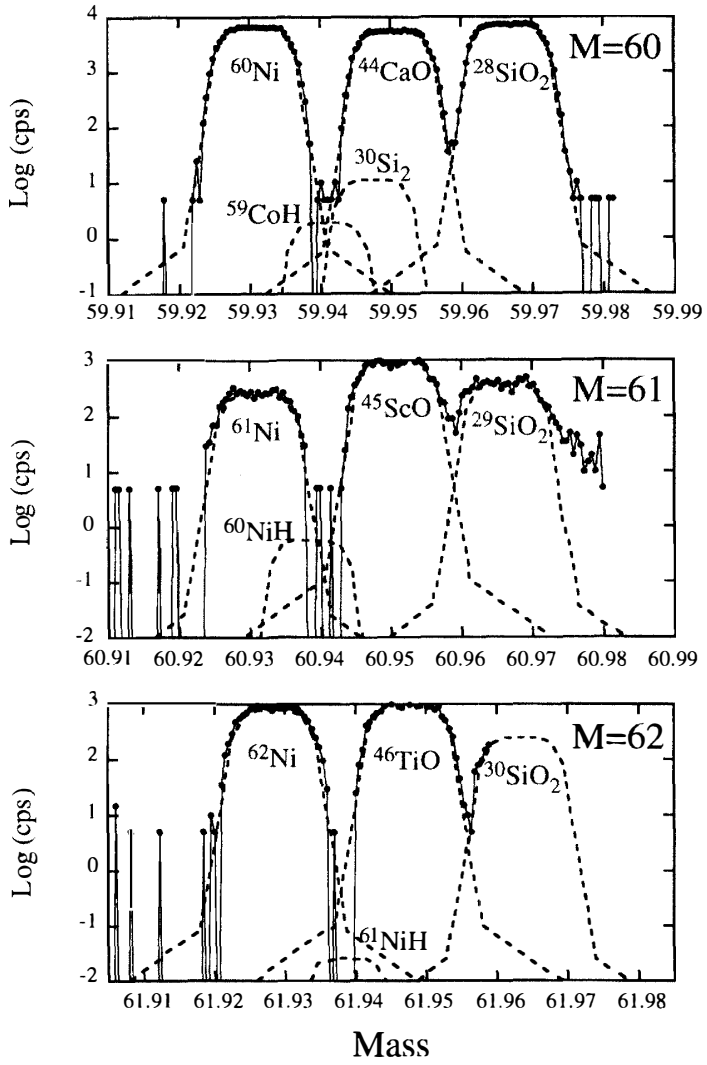

Fig. 1. Ni isotope mass spectra from the MET-78008 ureilite olivine core. The solid lines are measured mass spectra and the dashed lines represent fits to each ion. The hydride peaks were plot by assuming their peak heights to be 10^{-4} times of their metallic ions. The peak height of $^{30}Si_2$ is calculated from the peak height of $^{29}Si^{30}Si$ near ^{59}Co, which is not shown here.

ing of the mass peaks, which became critical for isotopic analyses.

The energy window was almost fully opened. In general, the instrumental isotopic mass fractionation factor depends on the initial energy of secondary ions (SLODZIAN *et al.*, 1980; HERVIG *et al.*, 1992; MORISHITA *et al.*, 1997). With the relatively high primary ion density, charging of the sample surface by the sputtering process may cause the shift in their energy distribution, so that the mass fractionation effect may vary during the isotopic analyses. In this work, gold coating of the sample is relatively thick (200 nm) in order to avoid sample charging. In addition, the wide energy window allows collection of nearly 100% of the ions passing through the energy slit of the mass spectrometer. Therefore, Ni isotope fractionation related to the initial eneregy of the secondary ions becomes insignificant.

2.3. Matrix effects on Ni abundance analyses

For trace element analysis by an ion microprobe, the energy filtering technique is commonly used (SHIMIZU *et al.*, 1978). As shown in Fig. 2, secondary ions detected in a mass spectrometer show a wide range of initial energy. The molecular ions show a narrower energy distribution than atomic ions. For this reason, in the energy filtering technique an offset voltage of −100 V is applied to the secondary accelerating voltage so that interferences of molecular ions are suppressed by the energy slit. Although the intensity of high energy ions is 1–2 order of magnitude lower than that of low energy ions, the technique has a great advantage because (1) matrix effects for sensitivity become insignificant for high energy ions, and (2) high mass resolution is not required.

In this study, we have examined matrix effects on Ni sensitivity relative to Fe using terrestrial olivine and orthopyroxene standards. We tested three different conditions with different ion energy bands; (1) no energy offset with an energy window of 20 V, (2) −100 V energy offset with an energy window of 20 V, and (3) no energy offset with large energy window of 75 V. The third condition is the one described in Section 2.2. The mass resolution defined by 10% peak height was 4500 for the conditions (1) and (3), and 2000 for the condition (2). Sensitivity factors of Ni relative to Fe (hereafter, SF(Ni/Fe)) shown in Fig. 3 increase with Fe contents in olivine. The matrix effect is less pronounced in the energy filtering mode (2), though more than 90% of the secondary ions were lost . We decided to use condition (3) for both abundance analyses and isotope

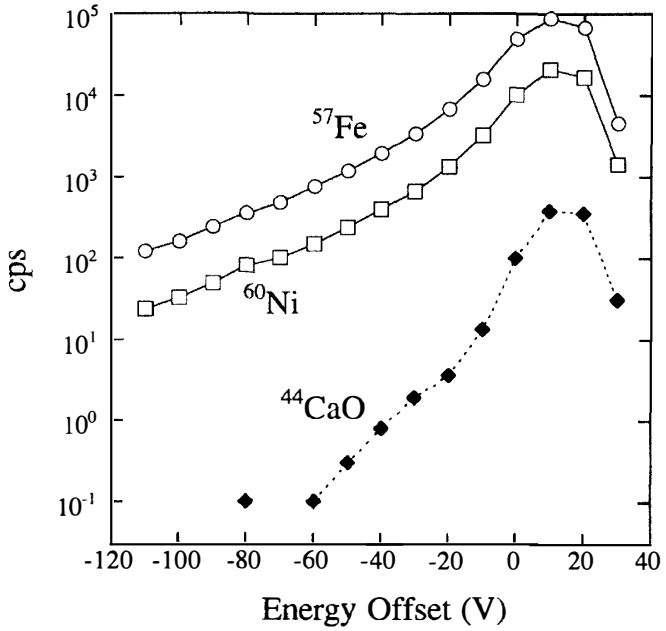

Fig. 2. Energy distribution of secondary ions. The energy spectrum was obtained by changing the secondary accelerating voltage (offset voltage). The energy window is 10 V.

analyses because the SF(Ni/Fe) can be calibrated within an error of 10%. The sensitivity factors SF(Co/Fe) vary in a similar manner to SF(Ni/Fe) between 0.6 and 1. For orthopyroxene, we had only one standard so that matrix effect could not be estimated. For ureilite orthopyoroxene analyses, we assumed SF(Ni/Fe)=0.5 and SF(Co/Fe)=0.6, which may introduce a small systematic error.

2.4. Ni isotope analyses of terrestrial standards

Isotopic analysis runs consist of 80 cycles of counting ^{60}Ni for 5 s, ^{61}Ni for 25 s, and ^{62}Ni for 8 s using an electron multiplier in a pulse counting mode, which takes an hour for a single analysis. The ^{60}Ni signal varied from 14000 cps in San Carlos olivine to 8000 cps in Orikabe olivine. In order to obtain ^{60}Ni/^{61}Ni ratios in the meteorite samples, the measured raw ratios of ^{60}Ni/^{61}Ni should be corrected for (1) dead time of the electron multiplier ion counting system, and (2) instrumental mass fractionation effects during the ion microprobe analyses. We have analyzed the Ni isotopic composition of terrestrial olivine standards for evaluation of these corrections.

The measured raw ratios of $(^{60}Ni/^{61}Ni)_{raw}$ and $(^{62}Ni/^{61}Ni)_{raw}$ are expressed in terms of the natural isotopic ratios $(^{60}Ni/^{61}Ni)_n$, $(^{62}Ni/^{61}Ni)_n$, $(^{61}Ni/^{60}Ni)_n$, and $(^{62}Ni/^{60}Ni)_n$, mass fractionation $(1+f)$, dead time of ion counting system τ, and Ni isotope count rates N(60), N(61), and N(62) as follows;

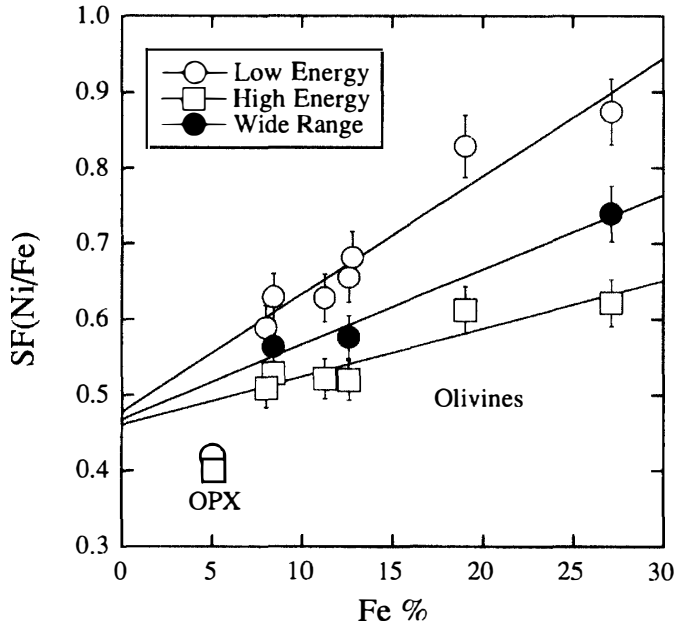

Fig. 3. Matrix effect on the secondary ion relative sensitivity factor of Ni and Fe. Sensitivity factors SF(Ni/Fe) were calculated by taking the ratio of measured ($^{60}Ni^+/^{56}Fe^+$) to the true ($^{60}Ni/^{56}Fe$) in a sample. The SF=1 indicates that the ionization efficiency of Ni is equal to that of Fe.

$$({}^{60}\mathrm{Ni}/{}^{61}\mathrm{Ni})_{\mathrm{raw}} = \frac{\mathrm{N}(60)\times\{1-\mathrm{N}(60)\times\tau\}}{\mathrm{N}(60)\times\{1-\mathrm{N}(61)\times\tau\}}\times(1-f)$$
$$\approx({}^{60}\mathrm{Ni}/{}^{61}\mathrm{Ni})_{\mathrm{n}}\times[1-f-\mathrm{N}(60)\times\tau\times\{1-({}^{61}\mathrm{Ni}/{}^{60}\mathrm{Ni})_{\mathrm{n}}\}], \quad (1)$$

$$\Delta({}^{60}\mathrm{Ni}/{}^{61}\mathrm{Ni})_{\mathrm{raw}} = \frac{({}^{60}\mathrm{Ni}/{}^{61}\mathrm{Ni})_{\mathrm{raw}}}{({}^{60}\mathrm{Ni}/{}^{61}\mathrm{Ni})_{\mathrm{n}}}-1$$
$$=-f-\mathrm{N}(60)\times\tau\times\{1-({}^{61}\mathrm{Ni}/{}^{60}\mathrm{Ni})_{\mathrm{n}}\}, \quad (2)$$

$$({}^{62}\mathrm{Ni}/{}^{61}\mathrm{Ni})_{\mathrm{raw}} = \frac{\mathrm{N}(62)\times\{1-\mathrm{N}(62)\times\tau}{\mathrm{N}(61)\times\{1-\mathrm{N}(61)\times\tau}\times(1+f)$$
$$\approx({}^{62}\mathrm{Ni}/{}^{61}\mathrm{Ni})_{\mathrm{n}}\times[1+f-\mathrm{N}(60)\times\tau\times\{({}^{62}\mathrm{Ni}/{}^{60}\mathrm{Ni})_{\mathrm{n}}-({}^{62}\mathrm{Ni}/{}^{60}\mathrm{Ni})_{\mathrm{n}}\}], \quad (3)$$

$$\Delta({}^{62}\mathrm{Ni}/{}^{61}\mathrm{Ni})_{\mathrm{raw}} = \frac{({}^{62}\mathrm{Ni}/{}^{61}\mathrm{Ni})_{\mathrm{raw}}}{({}^{60}\mathrm{Ni}/{}^{61}\mathrm{Ni})_{\mathrm{n}}}-1$$
$$=f-\mathrm{N}(60)\times\tau\times\{({}^{62}\mathrm{Ni}/{}^{60}\mathrm{Ni})_{\mathrm{n}}-({}^{61}\mathrm{Ni}/{}^{60}\mathrm{Ni})_{\mathrm{n}}\}. \quad (4)$$

In the above equations, we applied linear approximation for the dead time correction, while the exact formula of the dead time correction is as follows;

$$\mathrm{N}_{\mathrm{measure}}/\mathrm{N}_{\mathrm{true}} = \exp(-\mathrm{N}_{\mathrm{true}}\times\tau)\approx 1-\mathrm{N}_{\mathrm{true}}\times\tau. \quad (5)$$

By combining eqs. (2) and (4), the sum of $\Delta({}^{60}\mathrm{Ni}/{}^{61}\mathrm{Ni})_{\mathrm{n}}$ and $\Delta({}^{62}\mathrm{Ni}/{}^{61}\mathrm{Ni})_{\mathrm{n}}$ becomes the function of dead time only as follows;

$$\Delta({}^{60}\mathrm{Ni}/{}^{61}\mathrm{Ni})_{\mathrm{raw}}+\Delta({}^{62}\mathrm{Ni}/{}^{61}\mathrm{Ni})_{\mathrm{raw}} = -\mathrm{N}(60)\times\tau\times\{1-2\times({}^{61}\mathrm{Ni}/{}^{60}\mathrm{Ni})_{\mathrm{n}}+({}^{62}\mathrm{Ni}/{}^{60}\mathrm{Ni})_{\mathrm{n}}\}$$
$$=-\mathrm{N}(60)\times 1.051\times\tau. \quad (6)$$

Therefore, dead time τ is estimated by least square fitting of $[\Delta({}^{61}\mathrm{Ni}/{}^{60}\mathrm{Ni})_{\mathrm{raw}}+\Delta({}^{62}\mathrm{Ni}/{}^{60}\mathrm{Ni})_{\mathrm{raw}}]$ against ^{60}Ni count rate. As natural isotopic ratios for normalization, we used $({}^{60}\mathrm{Ni}/{}^{61}\mathrm{Ni})_{\mathrm{n}}=23.1000\pm0.0004$ and $({}^{62}\mathrm{Ni}/{}^{61}\mathrm{Ni})_{\mathrm{n}}=3.17596\pm0.00008$ from the literature values (BIRCK and LUGMAIR, 1988). As shown in Fig. 4, data plot along the linear trend and the slope of the line fit is $2.11\pm0.58\times10^{-5}$ ‰/cps, which corresponds to the dead time of 20±6 ns.

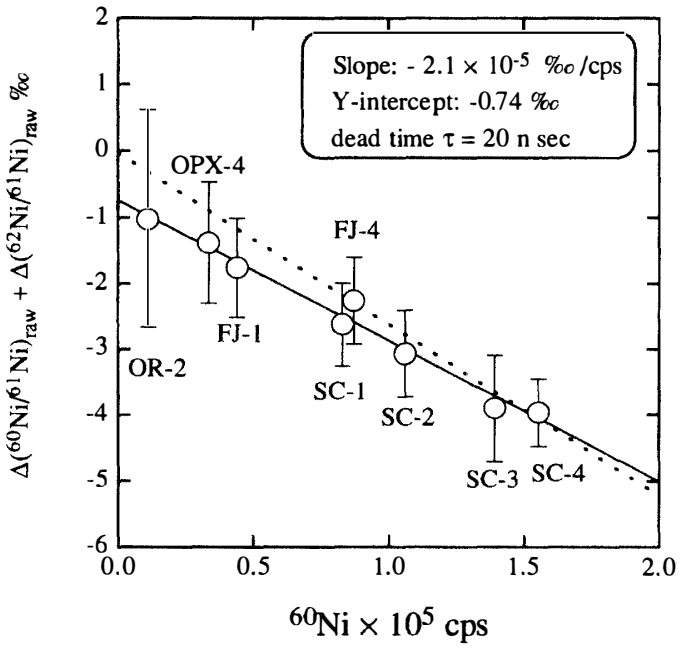

Fig. 4. Determination of the dead time of the ion counting system. Count loss of the major isotope ^{60}Ni in the ion detector causes deviations of the isotopic ratios. The sum of $\Delta(^{60}Ni/^{61}Ni)_{raw}+\Delta(^{62}Ni/^{61}Ni)_{raw}$ show the negative correlation with ^{60}Ni count rates. The dead time of the counter is calculated from the slope of the line. A small displacement of the Y-intercept from the origin indicates a small instrumental discrimination in our ion microprobe analyses compared to the literature Ni isotopic abundance obtained by thermal ionization mass spectrometer (Birck and Lugmair, 1988). The dashed line indicates the fit to the origin, which gives the dead time of 25±2 ns.

The Y-intercept of the Fig. 4 becomes (−0.74±0.63) ‰, indicating that there is a small discrepancy in our measured ratios from the literature values, which were obtained by high precision thermal ionization mass spectrometer analyses (Birck and Lugmair, 1988). If we force fit the data in Fig. 4 to the line passing through the origin (dotted line in the figure), three data points with lower count rates systematically shift below the line. Furthermore, this line fit gives the dead time of 25±2 ns, which is significantly larger than that obtained for other elements, such as O, Si, and Mg, between 18 and 21 ns (Kita, unpublished data). For these reasons, the discrepancy in our data from the literature values is significant. Tailing effects from the neighbor molecular interference may introduce systematic error for the sample with low Ni contents. We think it is unlikely because (1) the amount of tailing is always less than 10 ppm of the peak height and (2) the peak heights of molecular interference were monitored and found to be less than 10 times of the Ni isotopes, so that tailing effect does not introduce any systematic error more than 0.1‰. Actually, orthopyroxene has the largest molecular interference of CaO, ScO, and TiO relative to the Ni isotopes, though data are plotted on the same line within the errors.

Table 2. Results of ion probe Ni isotope analyses of terrestrial standards.

Samples†		^{60}Ni cps	$\Delta(^{62}Ni/^{61}Ni)$*		$\Delta(^{60}Ni/^{61}Ni)$*		$\delta(^{60}Ni)$§	
SC-96Nov	1	7.2E+4	0.85	± 1.07	-1.70	± 0.73	-0.85	± 1.29
	2	6.6E+4	2.42	± 1.06	-1.37	± 1.00	1.06	± 1.46
	3	5.8E+4	1.42	± 1.04	-0.76	± 0.90	0.66	± 1.37
	4	1.1E+5	1.92	± 0.81	-2.73	± 0.64	-0.81	± 1.03
	mean		1.69	± 0.49	-1.85	± 0.39	-0.16	± 0.63
SC-96Dec	5	1.4E+5	1.50	± 0.79	-1.63	± 0.88	-0.13	± 1.19
	6	9.2E+4	2.12	± 1.03	-1.51	± 0.91	0.61	± 1.37
	7	6.7E+4	2.84	± 1.04	-1.36	± 1.03	1.47	± 1.47
	8	1.1E+5	0.89	± 0.99	-2.51	± 0.79	-1.62	± 1.27
	mean		1.76	± 0.47	-1.83	± 0.45	-0.04	± 0.66
FJ-96Nov	9	4.3E+4	1.31	± 1.14	-2.82	± 0.99	-1.52	± 1.51
	10	4.4E+4	2.82	± 1.29	-0.99	± 1.09	1.83	± 1.69
	11	4.6E+4	1.51	± 0.87	-2.31	± 0.95	-0.80	± 1.28
	12	4.3E+4	2.92	± 1.25	-1.91	± 1.13	1.00	± 1.68
	mean		1.97	± 0.55	-2.07	± 0.52	-0.09	± 0.76
OR-96Dec	13	8.7E+3	-0.02	± 2.50	-5.03	± 2.20	-5.05	± 3.33
	14	1.2E+4	3.40	± 2.50	-0.51	± 2.18	2.89	± 3.31
	15	1.4E+4	1.95	± 2.26	-2.14	± 1.87	-0.19	± 2.93
	16	9.3E+3	3.85	± 2.81	-1.07	± 2.48	2.78	± 3.75
	mean		2.20	± 1.25	-2.23	± 1.07	-0.05	± 1.65
SC-97Feb	17	1.4E+5	-0.19	± 0.67	-0.51	± 0.76	-0.70	± 1.01
	18	1.4E+5	0.12	± 0.95	0.48	± 0.96	0.60	± 1.35
	mean		-0.08	± 0.55	-0.13	± 0.59	-0.23	± 0.81
SC-97Jun	19	1.4E+5	-1.59	± 0.66	0.77	± 0.60	-0.82	± 0.89
	20	1.8E+5	-0.33	± 0.60	1.17	± 0.66	0.84	± 0.89
	21	1.4E+5	-0.54	± 0.96	1.91	± 0.90	1.37	± 1.32
	22	1.6E+5	-1.52	± 0.89	0.53	± 0.87	-0.99	± 1.25
	mean		-0.95	± 0.37	1.04	± 0.36	0.05	± 0.52
FJ-97Jun	23	8.1E+4	-0.32	± 0.90	0.18	± 0.79	-0.14	± 1.19
	24	8.4E+4	0.13	± 0.77	0.08	± 0.73	0.21	± 1.06
	25	9.6E+4	1.10	± 0.87	-0.24	± 0.77	0.86	± 1.17
	mean		0.30	± 0.49	0.01	± 0.44	0.31	± 0.66
OPX-97Jun	26	3.0E+4	0.44	± 1.38	-1.23	± 1.37	-0.79	± 1.95
	27	3.7E+4	1.23	± 1.20	0.83	± 1.15	2.06	± 1.67
	28	3.0E+4	0.67	± 1.41	-1.09	± 1.29	-0.42	± 1.91
	29	3.6E+4	0.85	± 1.34	-1.99	± 1.25	-1.14	± 1.83
	mean		0.83	± 0.66	-0.77	± 0.63	0.06	± 0.91

† Sample names: SC- San Carlos olivine, FJ- Fuji olivines, OR- Orikabe olivines, OPX - Ichinomegata orthopyroxenes.

* The Ni isotopic ratios were shown as a permil deviation from the normalization values of $(^{62}Ni/^{61}Ni) = 3.17596$ and $(^{60}Ni/^{61}Ni) = 22.929$.

§ The $\delta(^{60}Ni)$ is corrected for mass fractionation using $\Delta(^{62}Ni/^{61}Ni)$.

In this work, we determined (^{60}Ni/^{61}Ni) ratios of the terrestrial standards from our ion microprobe analyses. The data were corrected for (1) a 20 ns dead time and (2) mass fractionation determined from the (^{62}Ni/^{61}Ni) ratios. The mean value of all the terrestrial standards was $(^{60}Ni/^{61}Ni)_c$=22.929±0.057. Therefore, in the following results, all the data are expressed as ‰ deviations, Δ(^{60}Ni/^{61}Ni) and Δ(^{62}Ni/^{61}Ni), from the normalization values of (^{60}Ni/^{61}Ni)=22.929 and (^{62}Ni/^{61}Ni)=3.17596, respectively.

The results of terrestrial standards are shown in Table 2 and an Ni three isotope plot in Fig. 5. All the data plot on a mass fractionation line within the analytical errors. The variation of Δ(^{62}Ni/^{61}Ni) obtained for different standards of different series of analyses in November 1996, December 1996, February 1997, and June 1997 is less than 3‰. For the standard analyses in June 1997, Au coating of the sample was 30 nm, which is thinner than before. We did not see any sample charging effects, such as deformation of ion image of the analyzing area, or shifts of energy spectrum of the secondary ions. However, the wider variation in Ni mass fractionation among different standards could have resulted from a small charging effect. For unknown samples with ^{60}Ni excess, data will be plotted above the mass fractionation line. Therefore, the ^{60}Ni excess is defined by δ (^{60}Ni) as follows;

$$\delta(^{60}Ni)=\Delta(^{60}Ni/^{61}Ni)+\Delta(^{62}Ni/^{61}Ni). \quad (7)$$

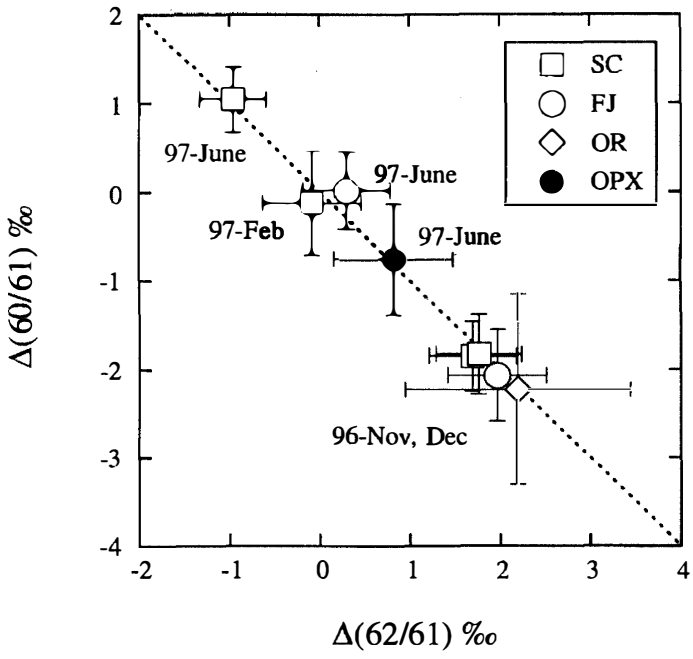

Fig. 5. Ni isotopic ratios of terrestrial standards. The data were corrected for the dead time of the ion counting system and expressed as permil (‰) deviations from the literature values. The dashed line represents the mass fractionation line. The data were obtained for different series of analyses of the following samples; SC=San Carlos olivine, FJ=Fuji olivine, OR=Orikabe olivine, OPX=orthopyroxene from Ichinome-gata nodule. The instrumental mass fractionation effect between different matrices and different analytical periods was smaller than ±2 ‰. The errors are $2\sigma_{mean}$.

2.5. MET-78008 ureilite sample

The sample of MET-78008 ureilite measured in this work was from the same specimen analyzed for the U-Pb age determination by TORIGOYE-KITA *et al.* (1995b). Olivine and low Ca-pyroxene grains of 0.3 - 1 mm size were used. These grains consist of homogeneous cores and reduced rims in contact with carbon-metallic veins. The thickness of the reduction rims is about 100 μm. Micron-sized Fe metal grains with low Ni contents (Ni <0.1%) are observed in the rim, which is produced by the reduction of FeO in olivine. Some of the low Ca pyroxene grains contain small metallic particles. The compositions of olivine and orthopyroxene are Fo=76 for core olivine, Fo=85 for reduced olivine near the rim, and En=76 for orthopyroxene (TORIGOYE-KITA *et al.* 1995b). We measured Ni isotopes and Fe/Ni and Fe/Co ratios of (1) core olivine, (2) core pyroxene, (3) olivine near the reduced rim, (4) low Ca pyroxene near metallic particles, and (5) a metallic grain in a carbon vein. Back scattered electron image of samples after ion microprobe analyses are shown in Fig. 6.

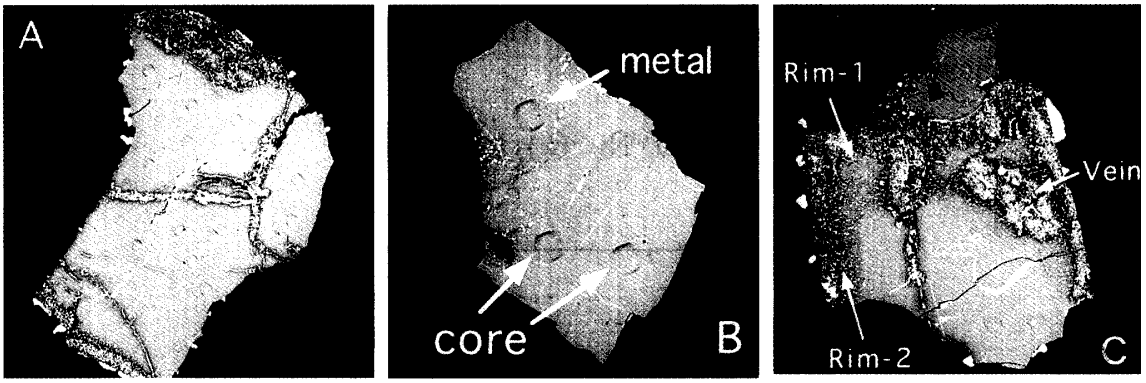

Fig. 6. Back scattered electron image of samples. The ion microprobe diameter is 40 μm. A: olivine grain 1 mm across. The spots are away from grain boundaries and show homogeneous Ni contents. B: orthopyroxene grain. One spot on the top contains a metallic inclusion, which was measured in this work. C: olivine grain near grain boundary. The back scattered electron image indicates reduction of Fe near the carbon-metal vein. Two spots from the rim region and one spot in the vein indicated by arrows were measured.

3. Results and Discussion

3.1. $^{60}Fe/^{56}Fe$ ratio at the time of ureilite formation

The results of Ni isotopic analyses and Co and Ni concentration analyses are shown in Table 3. Both Ni and Co contents of all samples, except the metallic phase in the vein, are lower than 100 ppm. The calculated $^{56}Fe/^{58}Ni$ ratios of silicate phases were between 2700 and 5400. These values are much higher than that of 190 from the bulk analysis of PCA 82506 ureilite (SHUKOLYUKOV and LUGMAIR, 1993b). Measured $^{59}Co/^{56}Fe$ and $^{60}Ni/^{56}Fe$ ratios of core olivine and pyroxene from the different spots are constant, which is consistent with a homogeneous chemical composition in the silicate cores. The Fe/Ni ratios of the reduced olivine rim were larger than those in the core by a factor of 2. At the beginning of each analysis, we examined sample ion images of the sputtering area.

Table 3. Results of ion probe analyses on the MET-78008 ureilite.

Sample		Ion Probe raw data					Corrected data ¶				
		^{60}Ni cps	$\Delta(^{62}Ni/^{61}Ni)$	$\Delta(^{60}Ni/^{61}Ni)$	$^{60}Ni^-/^{56}Fe^-$ $\times 10^{-5}$	$^{59}Co^-/^{56}Fe^-$ $\times 10^{-5}$	$\delta(^{60}Ni)$	$^{56}Fe/^{58}Ni$	Fe %	Ni ppm	Co ppm
Olivine core	G1-1	4403	1.36 ± 4.12	-4.90 ± 2.81	7.8	21.5	-3.54 ± 4.98		16.7	72	42
	G1-2	3867	3.45 ± 4.37	-1.27 ± 3.55	n.d.	n.d.	2.18 ± 5.63		16.7		
	G1-3	3391	4.37 ± 4.61	0.13 ± 3.70	7.2	21.1	4.51 ± 5.91		16.7	67	41
	G1-4	2470	3.93 ± 4.72	-6.88 ± 4.18	7.5	21.2	-2.95 ± 6.30		16.7	70	41
	G1-5	3096	2.62 ± 5.35	-3.62 ± 4.35	7.8	21.6	-1.00 ± 6.89		16.7	72	42
	G1-6	4227	-2.00 ± 3.89	-1.49 ± 3.31	8.1	n.d.	-3.49 ± 5.11		16.7	76	
	G1-7	2928	5.08 ± 4.58	-3.77 ± 3.87	7.8	n.d.	1.31 ± 6.00		16.7	72	
	G1-8	5116	0.76 ± 3.07	-0.88 ± 3.18	8.4	n.d.	-0.12 ± 4.42		16.7	78	
	G1-9	4246	0.85 ± 3.98	-4.49 ± 3.24	7.9	n.d.	-3.63 ± 5.14		16.7	73	
	G2-1	2610	2.23 ± 5.53	-4.47 ± 4.58	7.5	n.d.	-2.24 ± 7.18		16.7	70	
	G2-2	2533	2.94 ± 5.53	0.40 ± 4.64	6.5	n.d.	3.35 ± 7.22		16.7	60	
	G3-1	3332	3.33 ± 4.63	-0.81 ± 3.50	7.9	n.d.	2.52 ± 5.81		16.7	73	
	G3-2	2840	5.65 ± 3.53	-1.87 ± 3.53	7.6	n.d.	3.78 ± 4.99		16.7	71	
	mean		2.46 ± 1.18	-2.62 ± 1.00	7.7	21.4	-0.08 ± 1.56	3145	16.7	71	41
Reduced olivine rim	G3-3	1268	3.08 ± 8.36	6.74 ± 7.60	4.1	7.3	9.82 ± 11.30	5389	11.1	28	10
	G3-4	3293	3.98 ± 4.23	-4.35 ± 3.76	5.8	n.d.	-0.37 ± 5.66	4177	16.7	54	
Vein in olivine	G3-5	29475	-0.38 ± 1.59	1.24 ± 1.47	163	45	0.86 ± 2.17	100*			
Opx core	G4-1	1654	0.94 ± 6.61	-7.31 ± 5.38	3.8	n.d.	-6.37 ± 8.53		9.6	25	
G5-1	G5-1	1631	1.08 ± 6.54	-2.32 ± 4.79	3.9	16.1	-1.24 ± 8.11		9.6	26	24
G5-2	G5-2	1402	-0.15 ± 6.75	-5.56 ± 5.92	3.7	15.0	-5.71 ± 8.98		9.6	25	22
mean	mean		0.64 ± 3.83	-4.80 ± 3.06	3.8	15.6	-4.29 ± 4.92	5063	9.6	25	23
Opx with metal	G5-3	4854	0.88 ± 4.75	4.08 ± 3.68	7.0	16.7	4.96 ± 6.01	2740	9.6	46	25

¶ Concentration of Ni and Co were calculated using Fe contents in olivine (TORIGOE-KITA *et al.*, 1995b). * No matrix correction is applied to the Fe/Ni ratio. "n.d." indicates "not determined".

For the reduced olivine rim, we observed μm-sized metallic grains in the Fe and Ni images. Because Fe and Ni ionization efficiencies in metals are lower than those in silicates (KITA *et al.*, unpublished data), higher Fe/Ni ratios obtained from reduced olivine indicate that Ni in the olivine diffused into the metal much more than Fe during the reduction. Fe/Ni ratios of the vein could not be obtained quantitatively, because the sample is in a mixture of phases and its sensitivity factor is not known. However, measured $^{56}Fe/^{58}Ni$ ratio was 100, much lower than those of silicates, so that the vein may contain a significant amount of metallic particles with chondritic Fe/Ni ratios (30).

For the isotopic runs, the analytical error ($2\sigma_{mean}$) of single analyses was worse than 3‰ for all the silicate analyses because of low Ni contents. The precision of δ (^{60}Ni) after mass fractionation correction is worse than 5‰. The mean values of all analyses were obtained for olivine and orthopyroxene core data, because each mineral shows nearly constant Fe/Ni ratios. However, other data from grain boundaries showed variable Fe/Ni ratios so that data are shown for each point. The results are shown in Fig. 7 in a Ni three isotope plot. The olivine core mean value plots on the mass fractionation line, indicating that the Ni isotopic composition of olivine is normal within the errors. Other data seem to be scattered, though all of them are normal within analytical errors.

In Fig. 8, the δ (^{60}Ni) is plotted on a ^{60}Fe-^{60}Ni isochron diagram. None of the data shows a detectable excess. Linear regression of theses data to the line which passes through the origin gives the slope of $(-0.4\pm7.1)\times10^{-7}$. The upper limit of the slope cor-

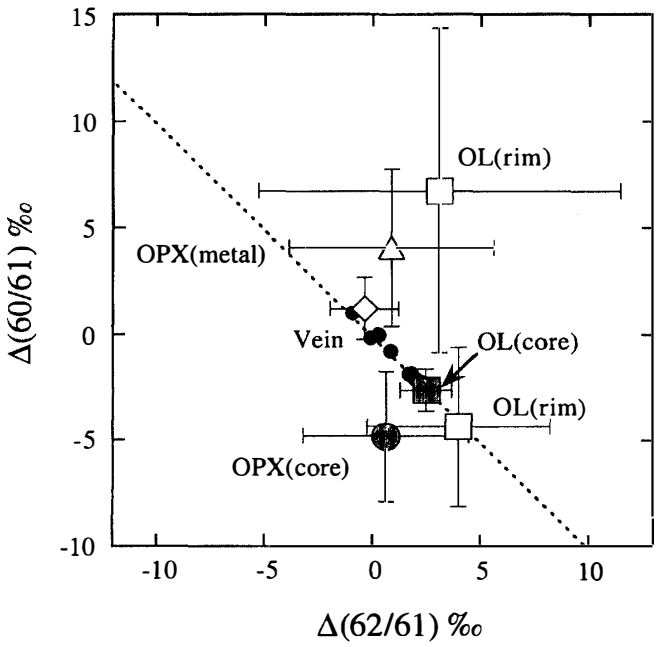

Fig. 7. The Ni isotopic abundance of silicate minerals and the vein of the MET-78008 ureilite. The dashed line indicates the mass fractionation line and the filled symbols are data from terrestrial standards. Considering the errors of the analyses, none of the results indicates a ^{60}Ni excess.

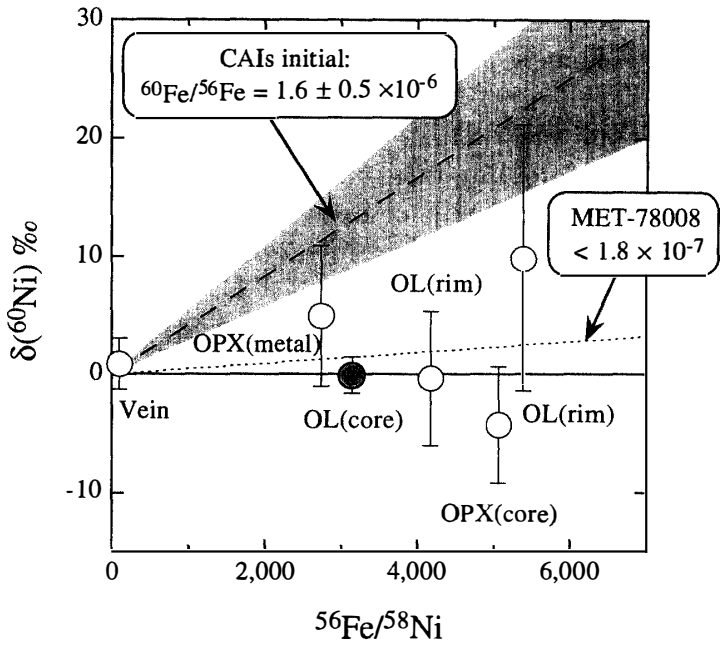

Fig. 8. *^{60}Fe-^{60}Ni isochron diagram for the MET-78008 ureilite. The broken line and shadowed area indicate the initial solar ^{60}Fe/^{56}Fe ratio inferred from CAIs (Birck and Lugmair, 1988). The upper limit of the ^{60}Fe/^{56}Fe ratio obtained from the core olivine analyses, 1.8×10^{-7}, is shown as a dashed line (see text).*

responds to initial ^{60}Fe/^{56}Fe ratio of 2.7×10^{-7}. The core olivine data with ^{56}Fe/^{58}Ni=3150 give δ (^{60}Ni)= −0.08±1.56‰, which is the most precise analysis. With these olivine data, an upper limit of ^{60}Fe/^{56}Fe < 1.8×10^{-7} is obtained. This upper limit and the initial abundance ratio of CAI (1.6±0.5×10^{-6}; Birck and Lugmair, 1988) imply a formation age interval between CAIs and MET-78008 of more than 3.9 million years.

A time interval of more than 4 million years is consistent with the time period required for the evolution of the initial Pb isotope composition in MET-78008, discussed by Torigoye-Kita *et al.* (1995b). The radiogenic U-Pb age of MET-78008 is 4.572±0.006 Ga if the Canõn Diablo Troilite Pb composition (CDT Pb; Tatsumoto *et al.*, 1973) is used as an initial Pb composition. The age is apparently older than the CAI formation age (4.566±0.002 Ga), indicating that the initial Pb isotopic composition in MET-78008 was more radiogenic. Torigoye-Kita *et al.* (1995b) argued that the U-Pb age becomes 4.563±0.006 Ga by using the slightly evolved Pb isotopic composition as an initial. This model calculation indicates that the Pb isotopes in the ureilite source region evolved from the CDT Pb composition for 3 million years with μ-value of 10 (Torigoye-Kita *et al.*, 1995b). Consequently, the formation interval between CAIs and the MET-78008 ureilite is 3±6 million years, or smaller than 9 million years. If we combine the results from the U-Pb system and the ^{60}Fe -^{60}Ni system, the ureilite might have been formed between 4 and 9 million years after the CAIs.

Here, we briefly summarize mineralogical evidence for the ureilite thermal history. The mineral chemistry of ureilite silicates indicates high equilibration temperature and

subsequent rapid cooling at lower temperatures. Generally, high CaO contents in ureilite olivine (up to 0.45%; GOODRICH, 1992) indicate a high temperature of equilibration (WASSON *et al.*, 1976). TAKEDA (1987) obtained a pyroxene equilibration temperature of 1250°C for both MET-78008 and Y-74130 ureilites using three pyroxene thermometers. They also obtained the rapid cooling rate of 20 °C/hr from a spinodal decomposition texture in augites. This cooling rate is comparable to the cooling rate estimates for various ureilites using reduction olivine rims (MIYAMOTO *et al.*, 1985). Therefore, ureilite must have experienced a rapid cooling history. For this reason, many authors suggest that ureilites experienced an impact event at the last stage of their evolution (TAKEDA, 1987; WARREN and KALLEMEYN, 1989, 1992). It is very likely that the Fe-Ni system in ureilite was closed soon after the impact event because of rapid cooling.

The interpretation of the lower limit of the formation interval (4 million years) depends on the behavior of siderophile elements during the mafic silicates formation. Mafic silicates are depleted in Ni (<100 ppm) so that Ni isotopes would be homogenized easily because of the co-existing Fe-Ni phases. If metallic phases were completely segregated from mafic silicates, data from the olivine core would indicate the time of metal segregation at the ureilite source. Because of high Fe/Ni ratios in bulk mafic silicates, ^{60}Ni excesses would be seen in all silicate fractions if the metal segregation occurred before ^{60}Fe had decayed. It is likely that the Ni isotopes in core olivine were not altered by the impact event and vein formation. Therefore, in the case that the metallic phases were completely segregated during the mafic silicate formation, the result from the olivine cores indicates that metal segregation did not occur earlier than 4 million years after the time of CAI formation.

However, it is not likely that metal phases were completely segregated from mafic silicates. Ureilite might have formed as a partial melting residue of chondritic precursor in a relatively small parent body (TAKEDA, 1987; WARREN and KALLEMEYN, 1989). Without high gravity and a large volume of silicate liquid, metallic phases would not be completely segregated. In some ureilites, small metallic spherules (<100 μm) have been observed in core olivine (BERKLEY *et al.*, 1980), indicating that FeNi-FeS components existed during the mafic silicate formation. Therefore, we believe that the ^{60}Fe-^{60}Ni system was open to metallic phases until the formation of carbonaceous veins. Therefore, both the U-Pb and ^{60}Fe-^{60}Ni systems might have been open during the subsolidus equilibration of silicates and became closed by the impact event when the carbonaceous veins were formed. Thus, the combination of two chronometer restricts the time of the impact event; between 4 and 9 million years after CAI formation.

3.2. The problem of initial ^{60}Fe/^{56}Fe ratio in the solar system

The discussion above is based on the assumption that the ^{60}Fe/^{56}Fe ratio at the time of CAI formation is $(1.6\pm0.5)\times10^{-6}$. However, it has not been fully confirmed whether the ^{60}Ni excess in CAIs were caused by the in-situ decay of live ^{60}Fe. The ^{60}Ni excess in CAIs is associated with isotopic anomalies of the neutron-rich isotopes ^{62}Ni and ^{64}Ni (BIRCK and LUGMAIR, 1988). The magnitude of the anomaly of all these isotopes are in the range between 0.1 and 0.3‰ after mass fractionation correction using the ^{61}Ni/^{58}Ni ratio. Isotope anomalies of other elements in CAIs are generally seen for the neutron-

rich isotopes, such as ^{48}Ca, ^{50}Ti, and ^{54}Cr. Therefore, BIRCK and LUGMAIR (1988) interpreted the ^{62}Ni and ^{64}Ni isotope anomalies to be of nucleosynthetic origin, while the ^{60}Ni excess to be of radiogenic origin. However, the correlation between ^{60}Ni excess and Fe/Ni abundance ratios has not been examined. Therefore, the ^{60}Ni excess could also have a nucleosynthetic origin and may not be caused by the ^{60}Fe decay. For this reason, the initial ^{60}Fe/^{56}Fe abundance of $(1.6\pm0.5)\times10^{-6}$ has a big uncertainly beyond its equoted error.

The first clear evidence of live ^{60}Fe in the solar system was found in the eucrites Chervony Kut and Juvinas with extremely high Fe/Ni ratios (SHUKOLYUKOV and LUGMAIR, 1993a; 1993b). A linear correlation was observed between excess ^{60}Ni and ^{56}Fe/^{58}Ni ratios for whole rock samples of each meteorite, though the mineral separates of Chervony Kut showed a significant disturbance. The ^{60}Fe/^{56}Fe ratio estimated from the isochron is $(3.9\pm0.6)\times10^{-9}$ for Chervony Kut and $(4.3\pm1.5)\times10^{-10}$ for Juvinas. These authors interpreted these ratios as the ^{60}Fe/^{56}Fe ratios at the time of crystallization of each eucrite. In order to estimate the initial ^{60}Fe/^{56}Fe ratios in the solar system from eucrite data, it is necessary to determine absolute ages of these eucrites by the U-Pb chronometer. Unfortunately, the U-Pb system of Chervony Kut has not been determined. The U-Pb age of Juvinas is reported to be 4.539±0.004 Ga by MANHÈS *et al.* (1984), though the result showed discordance at 1.9 Ga because of the impact event. If we use the Juvinus U-Pb age of 4.539±0.004 Ga and the ^{60}Fe/^{56}Fe ratio in this meteorite to calculate the ^{60}Fe/^{56}Fe ratio at the time of CAI formation (4.566±0.002 Ga), the estimated ^{60}Fe/^{56}Fe is between 10^{-5} and 10^{-7}, which is consistent with the CAI data. Although the ^{60}Fe/^{56}Fe ratio indicates a relative age difference of 5 million years between Chervony Kut and Juvinas, the ^{53}Mn-^{53}Cr system indicates less than a million year age difference (LUGMAIR *et al.*, 1994). It is likely that cooling history of the eucrite parent body affects their chronometers. Therefore, it is not possible to estimate the initial ^{60}Fe/^{56}Fe ratio from eucrite data with enough confidence.

SHUKOLYUKOV and LUGMAIR (1993b) found a small ^{60}Ni excess of 0.08±0.08 ‰ in troilite of the Ste. Marguerite H4 chondrite, indicating that the ^{60}Fe/^{56}Fe ratio at the time of metamorphism was in the range of 1×10^{-8}. The precise U-Pb age of phosphate separates from this chondrite is known to be 4.563 Ga, which is 3±2 million years after CAI formation (GÖPEL *et al.*, 1994). Applying the U-Pb age difference, the initial ^{60}Fe/^{56}Fe ratio of CAIs is estimated to be less than 2×10^{-7}. This estimate is an upper limit, though much lower than the estimate from the analyses of CAIs. If we take the lower initial ^{60}Fe/^{56}Fe ratios from this estimate, it is not possible to resolve a time difference between CAIs and ureilite formation from this work. However, the closure temperature of the Fe-Ni system in troilite may be much lower than that of the U-Pb system in phosphates, then the initial ^{60}Fe/^{56}Fe ratio estimate for H4 troilite may be too low.

It is very important to establish the initial ^{60}Fe/^{56}Fe ratio in the solar system. It is necessary to find high Fe/Ni phase in chondritic meteorites, which did not experience any secondary processes in the parent body. We believe that the ion microprobe is an useful tool to analyze such a sample.

4. Conclusions

In-situ Ni isotope analyses in olivine and pyroxene grains from the MET-78008 ureilite did not show any resolvable excess of ^{60}Ni. Using the average of olivine analyses, we obtain an upper limit of the ^{60}Fe/^{56}Fe ratio at the time of ureilite formation of 1.8×10^{-7}. If we assume the ^{60}Fe/^{56}Fe ratio of CAIs to be $(1.6 \pm 0.5) \times 10^{-6}$, our results indicate that the ureilite is younger than CAIs at least by 4 million years. This result is consistent with the U-Pb data obtained previously (TORIGOYE-KITA *et al.*, 1995b). The ureilite source region in their parent body might have been heated at 1200 °C until at least 4 million years after CAI formation. However, it should be mentioned that the conclusion depends on the interpretation of ^{60}Ni excess in CAIs and the estimate of the initial ^{60}Fe/^{56}Fe ratio of the solar system.

Acknowledgments

We thank the National Institute of Polar Research of Japan for providing the ureilite sample to us. We are indebted to Dr. Ernst ZINNER and anonymous reviewer for the careful review of the manuscript. We are grateful to Drs. Yasuko OKUYAMA-KUSUNOSE and Masumi MIKOSHIBA of the Geological Survey of Japan for providing us with rock samples for terrestrial olivine and orthopyroxene standards. We thank Dr. Mitsunobu TATSUMOTO of US Geological Survey for his continuous encouragement to one of the authors (N. T. K.) throughout this work.

References

BERKLEY, J.L., TAYLOR, G.J., KEIL, K., HARLOW, G.E. and PRINZ, M. (1980): The nature and origin of ureilites. Geochim. Cosmochim. Acta, **44**, 1579–1597.

BIRCK, J.L. and LUGMAIR, G.W. (1988): Nickel and chromium isotopes in Allende inclusions. Earth Planet. Sci. Lett., **90**, 131–143.

CLAYTON, R.N. and MAYEDA, T.K. (1988): Formation ureilite by nebular processes. Geochim. Cosmochim. Acta, **52**, 1313–1318.

GÖBEL, R., OTT, U. and BEGEMANN, F. (1978): On trapped noble gases in ureilites. J. Geophys. Res., **83**, 855–867.

GOODRICH, C.A. (1992): Ureilite: A critical review. Meteoritics, **27**, 327–352.

GÖPEL, C., MANHÈS, G. and ALLÈGRE, C.J. (1994): U-Pb systematics of phosphates from equilibrated ordinary chondrites. Earth Planet. Sci. Lett., **121**, 153–171.

HERVIG, R.L., WILLIAMS, P., THOMAS, R.M., SCHAUER, S.N. and STEELE, I.M. (1992): Microanalysis of oxygen isotopes in insulators by secondary ion mass spectrometry. Int. J. Mass. Spectrom. Ion Processes, **120**, 45–63.

HIGUCHI, H., MORGAN, J.W., GANAPATHY, R. and ANDERS, E. (1976): Chemical fractionation in meteorites - X. Ureilites. Geochim. Cosmochim. Acta, **40**, 1563–1571.

LUGMAIR, G.W., MACISAAC, Ch. and SHUKOLYUKOV, A. (1994): Small time differences recorded in differentiated meteorites (abstract). Meteoritics, **29**, 493–494.

MANHÈS, G., ALLÈGRE, C.J. and PROVOST, A. (1984): U-Th-Pb systematics of the eucrite "Juvinas": Precise age determination and evidence for exotic lead. Geochim. Cosmochim. Acta, **48**, 2247–2264.

MANHÈS, G., GÖPEL, C. and ALLÈGRE, C.J. (1988): Sytématique U-Pb dans les inclusions rèfractaires d"Allende: le plus vieux materiau solaire. Comptes rendus des Journées d'étude d'Action thématique prog. Planétol, ed. by M. C. FESTOU and D. CHABOD. Bensançon, 323–327.

MIYAMOTO, M., TAKEDA, H. and TOYODA, H. (1985): Cooling history of some Antarctic ureilites. Proc. Lunar

Planet. Sci. Conf., 16th, D116–D122 (J. Geophys. Res., **90** Suppl.).

MORISHITA, Y., SASAKI, A., KITA, N.T. and TOGASHI, S. (1997): Microanalysis for sulfur and oxygen isotopic ratios using SIMS (abstract). SIMS XI.

SHIMIZU, N., SEMET, M. and ALLÈGRE, C.J. (1978): Geochemical applications of quantitative ion-microprobe analysis. Geochim. Cosmochim. Acta, **42**, 1321–1334.

SHUKOLYUKOV, A. and LUGMAIR, G.W. (1993a): Live iron-60 in the early solar system. Science, **259**, 1138–1142.

SHUKOLYUKOV, A. and LUGMAIR, G.W. (1993b): ^{60}Fe in eucrites. Earth Planet. Sci. Lett., **119**, 159–166.

SLODZIAN, G. (1975): Looking at the collection efficiency problem through the ion microscope optics. Natl. Bur. Std. Spec. Publ., **427**, 33–61.

SLODZIAN, G., LORIN, J.C. and HAVETTE, A. (1980): Isotopic effect on the ionization probabilities in secondary ion emission. J. Physique, **41**, L555–L558.

TAKEDA, H. (1987): Mineralogy of Antarctic ureilites and a working hypothesis for their origin and evolution. Earth Planet. Sci. Lett., **81**, 358–370.

TANAKA, T., KAMIOKA, H. and YAMANAKA, K. (1988): A fully automated γ-ray counting and data processing system for INAA and analysis of rock reference samples. Chishitsu Chosajo Geppo (Bull. Geol. Surv. Jpn.), **39**, 537–557 (in Japanese with English abstract).

TATSUMOTO, M., KNIGHT, R.J. and ALLÈGRE, C.J. (1973): Time differences in the formation of meteorites as determined from the ratio of lead-207 to lead-206. Science, **180**, 1279–1283.

TORIGOYE-KITA, N., MISAWA, K. and TATSUMOTO, M. (1995a): U-Th-Pb and Sm-Nd isotopic systematics of the Goalpara ureilite: Resolution of terrestrial contamination. Geochim. Cosmochim. Acta, **59**, 381–390.

TORIGOYE-KITA, N., TATSUMOTO, M., MEEKER, G.P. and YANAI, K. (1995b): The 4.56 Ga U-Pb age of the MET 78008 ureilite. Geochim. Cosmochim. Acta, **59**, 4087–4091.

WARREN, P.H. and KALLEMEYN, G.W. (1989): Geochemistry of polymict ureilite EET83309, and a partially-disruptive impact model for ureilite origin. Meteoritics, **24**, 233–246.

WARREN, P.H. and KALLEMEYN, G.W. (1992): Explosive volcanism and the graphite-oxygen fugacity buffer on the parent asteroid(s) of the ureilite meteorites. Icarus, **100**, 110–126.

WASSON, J.T., CHOU, C-L., BILD, R.W. and BAEDECKER, P.A. (1976): Classification of and elemental fractionation among ureilites. Geochim. Cosmochim. Acta, **40**, 1449–1458.

(Received August 25, 1997; Revised manuscript accepted December 2, 1997)